High-Order-Mode-Pass Mode (De)Multiplexer with a Hybrid-Core Vertical Directional Coupler

Huang, Quandong; Chiang, Kin Seng

Published in:
Journal of Lightwave Technology

Published: 15/08/2019

Document Version:
Post-print, also known as Accepted Author Manuscript, Peer-reviewed or Author Final version

Published version (DOI):
10.1109/JLT.2019.2901372

Publication details:
Huang, Q., & Chiang, K. S. (2019). High-Order-Mode-Pass Mode (De)Multiplexer with a Hybrid-Core Vertical Directional Coupler. *Journal of Lightwave Technology*, *37*(16), 3932-3938. Article 8651291. Advance online publication. https://doi.org/10.1109/JLT.2019.2901372

Huang, Q., & Chiang, K. S. (2019). High-Order-Mode-Pass Mode (De)Multiplexer with a Hybrid-Core Vertical Directional Coupler. Journal of Lightwave Technology, 37(16), 3932-3938. [8651291]. https://doi.org/10.1109/JLT.2019.2901372.

High-Order-Mode-Pass Mode (De)Multiplexer with a Hybrid-Core Vertical Directional Coupler

Quandong Huang and Kin Seng Chiang, *Member, IEEE, Fellow, OSA*

***Abstract*—We propose a high-order-mode-pass mode (de)multiplexer based on the structure of a vertical waveguide directional coupler formed with a few-mode core and a single-mode core that has a higher refractive index. Unlike a conventional directional coupler, where the two cores have the same refractive index, the hybrid-core structure allows the design of a directional coupler to couple only the fundamental mode of a few-mode core to a single-mode core without affecting the high-order modes of the few-mode core. To demonstrate the idea, we design and fabricate a vertical coupler formed with a three-mode core and a single-mode core with polymer material. Our experimental device has a length of 15 mm and a coupling ratio for the fundamental mode varying from 92.5% to 98.7% in the C-band (from 1530 to 1565 nm), which corresponds to a relative residual power of the fundamental mode in the three-mode core varying from −10.9 to −18.9 dB. The crosstalks to the single-mode core from the two high-order modes of the three-mode core are smaller than −13.8 dB in the C-band. The performance of the device is polarization-insensitive. The proposed hybrid-core mode (de)multiplexer allows an effective control of the fundamental mode of a few-mode waveguide and thus opens up new possibilities for the design of mode-controlling devices, such as mode-group (de)multiplexers, mode-dependent-loss compensators, and mode add-drop multiplexers, for mode-division-multiplexing applications based on circular or elliptical few-mode fibers.**

***Index Terms*—Integrated optics devices, multiplexing, optical polymer, optical waveguide components, optical waveguide couplers.**

I. Introduction

MODE-division multiplexing (MDM), which allows different spatial modes or mode groups of a few-mode fiber to carry different WDM signals, is an emerging technology for increasing the fiber communication capacity [1]–[5]. Recently, a signal-carrying capacity of 10.16 Peta-b/s has been demonstrated with a 6-mode 19-core fiber over a distance of 11.3 km, where each mode supports 739 WDM channels in the (C+L)-band using 12-Gbaud dual-polarization combined 64-QAM/16-QAM signals [6]. This transmission capacity is approximately 100 times of the limit of a single-mode fiber (SMF) (~100 Tb/s) [2]. A key component in an MDM system is a mode (de)multiplexer, which serves to combine (separate) different mode channels at the input (output) end of the system. A number of mode (de)multiplexers have been demonstrated with bulk-optics components [7]–[9], fibers [10]–[13], and waveguides [14]–[18] (see also the review paper [3]). Among these technologies, the waveguide technology offers much flexibility in material choice and structure design, which allows the realization of more powerful devices. Waveguide devices are compact and can be integrated to achieve more advanced functions. Conventional waveguides, however, are co-planar (or 2D) structures and this poses significant restrictions in the design of (de)multiplexers for fiber modes, which have 3D spatial distributions. For example, a co-planar directional coupler (DC) formed with two parallel waveguide cores in the horizontal direction only allows (de)multiplexing of two modes that have the same symmetry in the vertical direction; it does not allow (de)multiplexing of two modes that have opposite symmetries in the vertical direction. The mode-symmetry issue for mode-selective couplers has been analyzed in detail with fiber couplers for different combinations of mode orientations [19]. This problem can be solved by using a mode rotator to change the symmetry of the mode, where the mode rotator can be a precisely designed trenched waveguide [16] or an asymmetric long-period waveguide grating [18]. With this approach, a six-mode (de)multiplexer has been realized with eight horizontal DCs and two-mode rotators [17]. A more natural way to (de)multiplex fiber modes is to employ 3D waveguide structures, which allow the propagation of light in waveguides formed in different geometric levels. 3D three-mode (de)multiplexers that combine horizontal and vertical waveguide DCs have been fabricated with polymer by spin-coating and photolithography [20]–[22] or with boro-aluminosilicate glass by direct laser writing [23]. By combining 2D and 3D waveguide branches, ultra-broadband three-mode and four-mode (de)multiplexers that can operate over the entire (C+L)-band has been fabricated with polymer waveguides [24]. By using five cascaded vertical polymer waveguide DCs, a six-mode (de)multiplexer has been realized [25]. 3D thermo-optic mode switches for reconfigurable MDM systems have also been demonstrated [26]–[28].

In all the reported designs of mode (de)multiplexers based on asymmetric DCs [16],[17],[20]–[23],[25], the two waveguide cores that form the DC have the same refractive index. These designs provide effective mode (de)multiplexing

Manuscript received xx 2018. This work was supported by the Research Grants Council of the Hong Kong Special Administrative Region, China, under Project CityU 11253316. *(Corresponding author: Kin Seng Chiang.)*

All authors are with the Department of Electronic Engineering, City University of Hong Kong, 83 Tat Chee Ave., Kowloon, Hong Kong SAR, China (e-mail: qd.huang@my.cityu.edu.hk; eeksc@cityu.edu.hk).

by coupling the high-order modes of a few-mode core (FMC) into various single-mode cores (SMCs) and vice versa, with the fundamental mode of the FMC unaffected. However, there are devices, such as mode add-drop multiplexers, that require the fundamental mode of an FMC to be coupled to an SMC without affecting the high-order modes. While this function can be achieved with a grating-assisted asymmetric DC [29], the requirement of a strong grating in such a device introduces a large background loss to the high-order modes of the FMC and the use of a grating also limits the bandwidth of the device. Another technique is to reduce the effective index of the fundamental mode of an FMC in a DC by increasing the temperature of the FMC with an electrode heater deposited on its surface, but the electric power required for activating such a DC is high [30].

In this paper, we propose a DC formed with an FMC and an SMC that has a higher refractive index. Such a hybrid-core DC can be designed to couple the fundamental mode of an FMC to an SMC without affecting the high-order modes of the FMC. Because of the constraints in the fabrication process, a hybrid-core DC should rather be realized with a vertical DC instead of a horizontal DC. To demonstrate the principle, we design a vertical hybrid-core DC formed with a three-mode core and an SMC to couple between the fundamental modes of the two cores, i.e., to function as a high-order-mode-pass mode (de)multiplexer. We fabricate the device with polymer material to take advantage of the spin-coating process available to form multilayer waveguide structures. Our experimental device provides a coupling ratio for the fundamental mode varying from 92.5% to 98.7% in the C-band with low polarization dependence. The crosstalks to the SMC from the two high-order modes of the three-mode core are smaller than −13.8 dB in the C-band. The hybrid-core DC structure can serve as a platform for the realization of a wide range of mode-controlling devices, such as mode-group (de)multiplexers, mode add-drop multiplexers, mode filters, and mode-dependent-loss compensators, which require the control of the fundamental mode of a few-mode waveguide.

II. Operating Principle and Design

A schematic diagram of the cross section of a conventional vertical DC formed with an FMC and a parallel SMC placed above is shown in Fig. 1(a), where the two cores have the same refractive index. As the two cores have the same refractive index, the effective index of the fundamental mode (i.e., the E_{11} mode) of the larger FMC is always larger than that of the smaller SMC. Therefore, it is impossible to use such a DC to achieve strong coupling between the fundamental modes of the two cores, because the phase-matching condition cannot be satisfied. Such a DC, however, can be designed to couple a high-order mode of an FMC to an SMC by matching their effective indices [20]–[22],[25],[28], as shown by the example in Fig. 1(b). To achieve strong coupling between the fundamental modes of an FMC and an SMC, we propose using a hybrid-core vertical DC, where the refractive index of the FMC is smaller than that of the SMC, as shown in Fig. 1(c). By decreasing the effective index of the fundamental mode of the FMC through using a smaller refractive index for the FMC, it becomes possible to match the effective indices of the fundamental modes of the two cores, as shown in Fig. 1(d), and thus achieve strong coupling between them without affecting the high-order modes of the FMC.

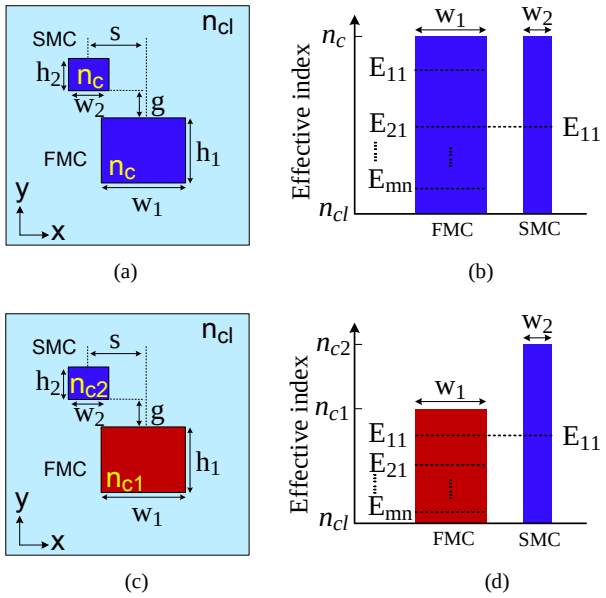

Fig. 1. (a) Cross section of a conventional vertical DC formed with an FMC and an SMC, where the two cores have the same refractive index n_c; (b) phase-matching diagram for a conventional vertical DC, where the effective index of the E_{21} mode of the FMC (which supports the E_{11}, E_{21}, …, E_{mn} modes) is equal to the effective index of the E_{11} mode of the SMC; (c) cross section of a hybrid-core vertical DC formed with an FMC and an SMC, where the refractive index of the FMC n_{c1} is smaller than that of the SMC n_{c2}; and (d) phase-matching diagram for a hybrid-core vertical DC, where the effective indices of the E_{11} modes of the two cores are equal. In the above figures, w_1 and w_2 denote the widths of the FMC and the SMC, respectively; h_1 and h_2 denote the heights of the FMC and the SMC, respectively; s and g denote the horizontal and vertical separations of the two cores, respectively, and n_{cl} denotes the refractive index of the cladding that surrounds the cores.

Here we present a design of a hybrid-core vertical DC for achieving strong coupling between the E_{11} modes of an FMC and an SMC without affecting the high-order modes of the FMC, i.e., a high-order-mode-pass mode (de)multiplexer. Figure 2 is a schematic diagram of the device, where the hybrid-core DC is formed with an FMC (Core 1) located in the lower layer and an SMC (Core 2) located in the upper layer. The FMC supports three modes, namely the E_{11}, E_{21}, and E_{12} modes, and the SMC supports only the E_{11} mode. Two cosine-shaped S-bends are introduced along the SMC to separate the two cores at the two ends of the device. Our goal is to determine the parameters of the device, so that the E_{11} mode launched into Core 1 is coupled to Core 2 as much as possible, while the E_{21} and E_{12} modes launched into Core 1 mainly stay in Core 1.

We calculate the effective indices of the modes of the individual cores with a mode solver based on the full-vector finite-element method (COMSOL) and search for the phase-matching condition for the E_{11} modes of the two cores. The refractive indices of Core 1, Core 2, and the cladding are taken to be n_{c1} = 1.564, n_{c2} = 1.569, and n_{cl} = 1.559, which

correspond to the refractive indices of the polymer materials used in our fabrication work. There are many possible designs. We fix the heights of Core 1 and Core 2 at h_1 = 11.0 μm and h_2 = 4.0 μm. The variations of the effective indices of different modes with the widths of Core 1 (w_1) and Core 2 (w_2), calculated for the TE polarization at the wavelength 1550 nm, are shown in Fig. 3(a). To guarantee single-mode operation for Core 2, the width of Core 2 must be smaller than 7.0 μm. In our design, we choose w_1 = 13 μm and w_2 = 5.2 μm, so that the effective indices of the E_{11} modes of the two cores have the same value (1.5625), i.e., the two modes satisfy the phase-matching condition. The intensity patterns of the modes of Core 1 and Core 2, calculated for the chosen core dimensions, are shown in Fig. 3(b) and 3(c), respectively. As the effective indices of the E_{21} and E_{12} modes of Core 1 are much smaller than that of the E_{11} mode, the couplings from the E_{12} and E_{21} modes of Core 1 to Core 2 should be weak. As the difference between the effective indices of the TE and TM polarizations is small ($<10^{-5}$), the performance of the device is expected to be polarization-insensitive. The coupling length of the DC for the E_{11} modes of the two cores depends on the values of the horizontal and vertical core separations s and g. In our design, we choose s = 5.5 μm and g = 3.0 μm. By performing wave propagation along the DC with a 3D finite-difference beam propagation method (BPM) (3DFD-BPM, RSoft), we can determine the length of the DC.

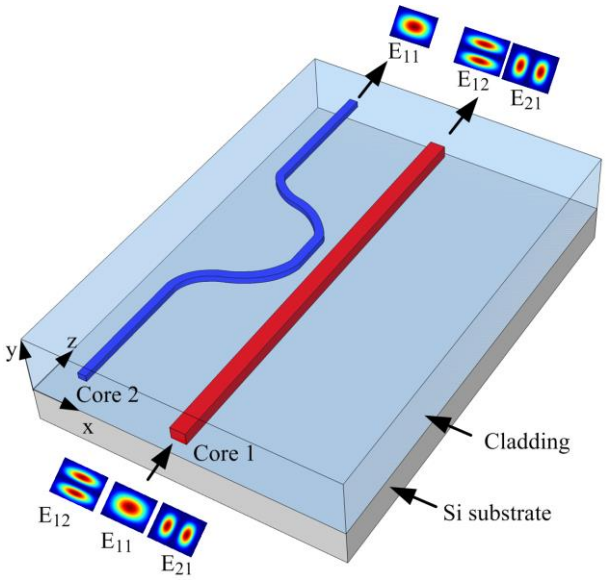

Fig. 2. Structure of the proposed high-order-mode-pass mode (de)multiplexer, which consists of a hybrid-core vertical DC formed with a low-index three-mode core (Core 1) located in the lower layer and a high-index SMC (Core 2) located in the upper layer.

Figure 4(a) shows the top view of our final design obtained by BPM simulation and Fig. 4(b), 4(c), and 4(d) show the simulated propagation results at 1550 nm for the E_{11}, E_{21}, and E_{12} modes launched into Core 1 individually. As shown in Fig. 4(a), the length of the parallel section of the two cores is 1.72 mm and each S-bend has a length of 3 mm, which separates the two cores by 50 μm at each end. As shown in Fig. 4(b), almost all of the input power of the E_{11} mode launched into Core 1 is coupled to Core 2, while, as shown in Fig. 4(c) and 4(d), the coupling from the E_{21} or E_{12} mode of Core 1 to Core 2 is negligible. The hybrid-core vertical DC functions as an effective high-order-mode-pass mode (de)multiplexer, where only the E_{11} mode of Core 1 is coupled effectively to Core 2.

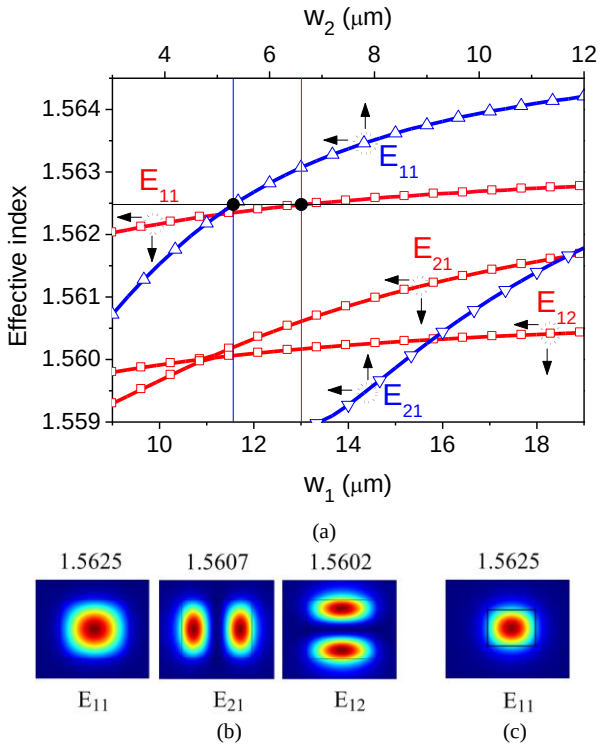

Fig. 3. (a) Variations of the effective indices of different TE-polarized modes with the widths of Core 1 (w_1) (red squares) and Core 2 (w_2) (blue triangles) at 1550 nm with the heights of Core 1 and Core 2 fixed at 11 and 4 μm, respectively, where the thin vertical lines highlight the chosen widths for Core 1 (w_1 = 13 μm) and Core 2 (w_2 = 5.2 μm) for satisfying the phase-matching condition. The intensity patterns of the TE-polarized modes of (b) Core 1 and (c) Core 2 calculated for the core widths w_1 = 13 μm and w_2 = 5.2 μm at 1550 nm, where the numbers above the patterns are the effective indices of the corresponding modes.

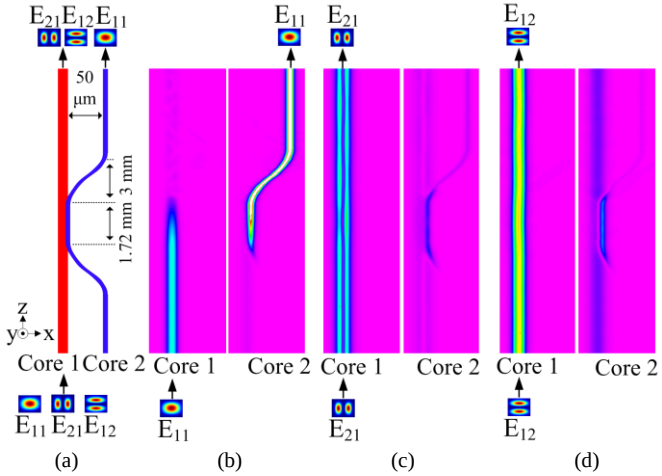

Fig. 4. (a) Top view of our design obtained by BPM simulation. Simulated propagation results at 1550 nm for the TE-polarized (b) E_{11}, (c) E_{21}, and (d) E_{12} modes launched into Core 1 individually.

The device is characterized by the coupling ratios CR_{mn} for the E_{mn} (mn = 11, 21, and 12) modes of Core 1, which are expressed as

$$CR_{mn} = \frac{P_{out-mn}}{P_{out-total}}, \quad (1)$$

where $P_{out\text{-}mn}$ is the output power from Core 2, when the E_{mn} mode is launched into Core 1, and $P_{out\text{-}total}$ is the total output power from Core 1 and Core 2. The simulation results for the coupling ratios CR_{11}, CR_{21}, and CR_{12} for the TE and TM polarizations over the C-band (1530 – 1565 nm) are shown in Fig. 5. The coupling ratio CR_{11} is higher than 95.1% (96.0%) for the TE (TM) polarization in the C-band with a maximum value of 99.99% at 1550 nm, while the coupling ratios CR_{21} and CR_{12} are lower than 0.09% (0.10%) and 0.02% (0.02%) for the TE (TM) polarization in the C-band, respectively.

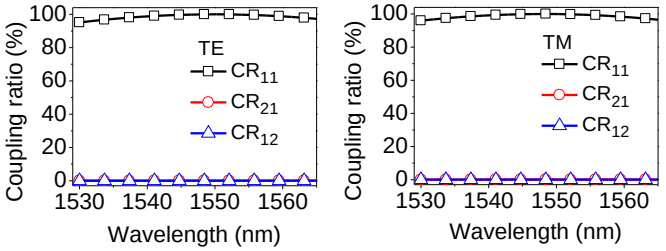

Fig. 5. Simulation results for the coupling ratios CR_{11}, CR_{21}, and CR_{12} for the TE and TM polarizations.

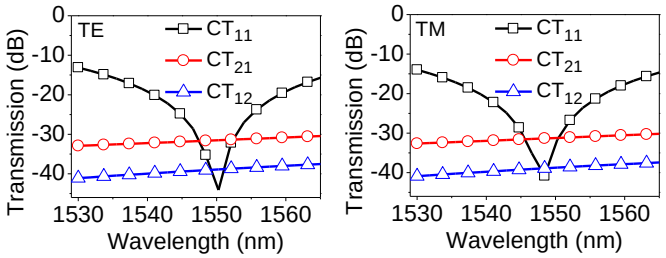

Fig. 6. Simulation results for the modal crosstalks CT_{11}, CT_{21}, and CT_{12} for the TE and TM polarizations.

The residual power of the E_{11} mode in Core 1 represents the crosstalk to the other two modes. With $(1 - CR_{11}) << 1$, the crosstalk caused by the residual power of the E_{11} mode in Core 1 can be approximated by $CT_{11} = 10 \log (1 - CR_{11})$ (in dB). Similarly, the powers coupled to Core 2 from the E_{21} and E_{12} modes of Core 1 represent the crosstalks to the E_{11} mode. With $CR_{21} << 1$ and $CR_{12} << 1$, the crosstalks caused by the E_{21} and E_{12} modes to the E_{11} mode can be approximated by $CT_{21} = 10 \log CR_{21}$ and $CT_{12} = 10 \log CR_{12}$ (in dB), respectively. The simulation results for the crosstalk characteristics of the device for the TE and TM polarizations are shown in Fig. 6. The crosstalks CT_{11}, CT_{21}, and CT_{12} in the C-band are smaller than −13.1 (−13.9), −30.5 (−30.2), and −37.5 (−37.4) dB for the TE (TM) polarization. The minimum value of CT_{11} (−44.1 dB) is obtained at 1550 nm for the TE polarization. As shown in Fig. 3(a), a small change in the width of Core 1 at the chosen width value does not lead to a significant change in the effective index of the E_{11} mode. Our design has good tolerance on the width of Core 1. A variation of the width of Core 2 gives rise to a larger effect on the device performance. Nevertheless, with a variation of the width of Core 2 by ±0.3 μm, the coupling ratio CR_{11} at 1550 nm is still larger than 80% and the crosstalk CT_{21} (CT_{12}) is smaller than −30 (−37) dB. As confirmed by the results in Fig. 5 and Fig. 6, the characteristics of the device are polarization-insensitive.

III. Device Fabrication

We fabricated the proposed hybrid-core DC by following the design parameters with our in-house micro-fabrication facilities. The waveguide materials used were UV-curable polymer materials EpoCore and EpoClad (Micro Resist Technology GmbH). Pure EpoCore and pure EpoClad were used as the materials for Core 2 and the cladding, respectively, and a mix of equal amounts of EpoCore and EpoClad was used as the material for Core 1. The refractive indices of the materials for Core 1, Core 2, and the cladding, measured with thin-film samples at the wavelength 1536 nm with a prism coupler (Metricon 2010), were 1.564, 1.569, and 1.559, respectively. The refractive-index difference between the TE and TM polarizations is smaller than 0.001.

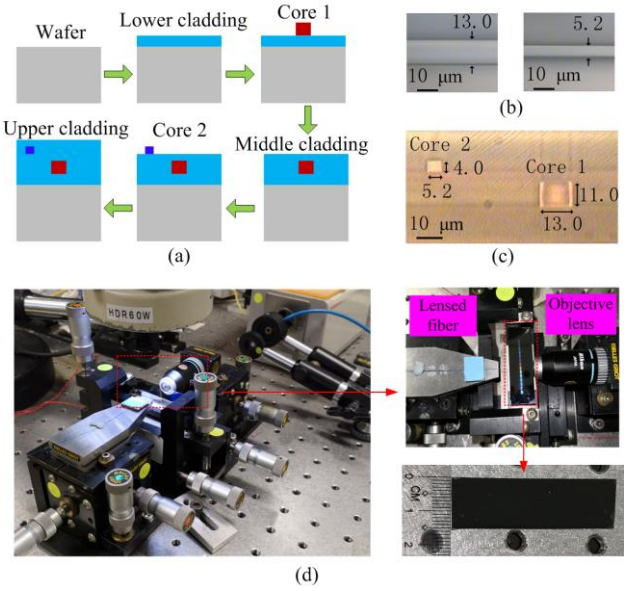

Fig. 7. (a) Steps in the fabrication of the proposed hybrid-core DC with polymer materials; (b) photos showing the top views of Core 1 (left) and Core 2 (right) of a fabricated device; (c) photo showing an end face of the fabricated device; and (d) photos of the measurement setup and the device on the chip under test.

The steps in the fabrication of the device are summarized in Fig. 7(a). The fabrication process starts with the preparation of a clean substrate, which is a 3-inch 100-orientation silicon wafer treated by reactive-ion etching (RIE). A layer of EpoClad is first spin-coated onto the substrate to form a thick (>15 μm) lower cladding. A layer of the mixed polymer material for Core 1 is then spin-coated onto the lower cladding and patterned by the standard photolithography process with a mask that defines the width of the core. The thickness of the core formed by spin-coating is made slightly larger than the

design value, so that it can be trimmed to the exact design value by RIE. A layer of EpoClad is next spin-coated onto the sample to form the middle cladding, whose thickness is trimmed to the desired value with RIE. By following the same steps used in forming Core 1, Core 2 is formed on top of the middle cladding with EpoCore and another mask and trimmed to the design height with RIE. The main challenge in the fabrication of a vertical coupler is the alignment of the cores in different layers. We solve this problem by introducing precise alignment markers on the masks that define the core patterns in the two layers. Finally, another layer of EpoClad is spin-coated onto the sample to form a thick (>15 μm) upper cladding. Each spin-coated polymer film is fully cured before it is further processed. The length of the whole device, which includes the waveguide leads at both ends, is about 15 mm. Figure 7(b) are photos of the top views of Core 1 and Core 2 of a fabricated device and Fig. 7(c) is a photo showing an end face of the device, where the dimensions of the cores were measured with a step profiler (AMBIOS XP-2) and an optical microscope (Leica DM 2500 M) during the fabrication. The dimensions of the cores at the two ends are the same, so there is no differentiation between the two ends in terms of the operation of the device.

With our fabrication facility, the uncertainties in the control of the width and the height of the cores are about ±0.3 μm and ±0.1 μm (after RIE trimming), respectively. To solve the tolerance problem, we fabricated a series of devices with core widths varying from the nominal value by ±0.4 μm at a step of 0.1 μm on the same substrate and selected the one that gave the best performance for demonstration.

IV. Device Characterization

Figure 7(d) are photos of the measurement setup and the device on the chip under test. To evaluate the performance of the fabricated device, we launched the E_{11}, E_{21}, and E_{12} modes individually into Core 1 at one end of the device with a pigtailed C-band tunable laser (KEYSIGHT) and captured the corresponding output near- field images from both cores at the other end with an infrared camera. The E_{21} and E_{12} modes were selectively excited by properly adjusting the position and the tilt angle of the laser beam incident onto Core 1 via a lensed fiber with the help of a five-degree micro-positioner. The near-field images shown in Fig. 8(a) confirm that the E_{11} mode launched into Core 1 is coupled almost completely to Core 2, while the E_{21} and E_{12} modes launched into Core 1 stay in Core 1. When we launched the E_{11} mode into Core 2, we observed almost complete coupling from Core 2 to the E_{11} mode of Core 1, as shown in Fig. 8(b). As expected, this device functions as an effective high-order-mode-pass mode (de)multiplexer with only the E_{11} mode of Core 1 coupled to Core 2. There is no significant difference in the device performance between the two polarizations.

In addition to taking near-field images, we measured the output powers from Core 1 and Core 2 with a power meter (Newport 2832-C) via a 40X objective lens to evaluate the coupling ratios and the crosstalks of the device. For the power measurements, we launched the E_{11} mode into Core 2 (to ensure mode purity) and the E_{21} and E_{12} modes into Core 1 individually. From the measured output powers, we calculated the coupling ratios for the E_{11}, E_{21}, and E_{12} modes from Eq. (1). The results obtained for the TE and TM polarizations are shown in Fig. 9. In the C-band, the coupling ratios CR_{11} is higher than 94.3% (92.5%), while the coupling ratios CR_{21} and CR_{12} are lower than 3.1% (4.0%) and 2.7% (2.9%) for the TE (TM) polarization.

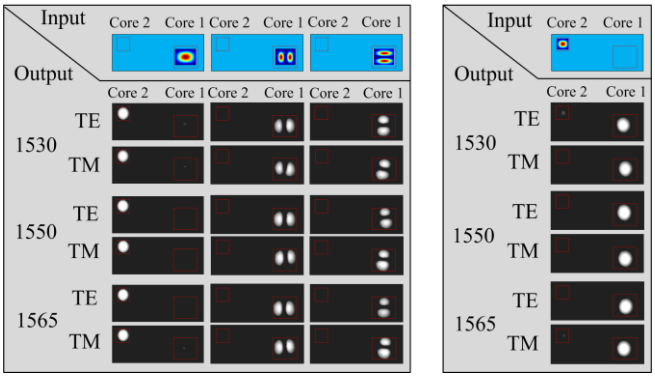

Fig. 8. Output near-field photos taken from Core1 and Core 2 at 1530, 1550, and 1565 nm for the TE and TM polarizations, (a) when the E_{11}, E_{21}, and E_{12} modes were launched into Core 1 individually, and (b) when the E_{11} mode was launched into Core 2.

Figure 10 shows the modal crosstalks obtained from the power measurements. In the C-band, the crosstalks CT_{11}, CT_{21}, and CT_{12} are lower than −12.2 (−10.9), −14.9 (−13.8), and −15.5 (−15.2) dB for the TE (TM) polarization.

We should note that, in practice, it is difficult to launch a pure high-order mode into Core 1. The unavoidable excitation of a small amount of the E_{11} mode in optimizing the launching of a high-order mode into Core 1 contributes to the values of CR_{21}, CR_{12}, CT_{21}, and CT_{12} obtained from the power measurements. The actual values of CR_{21}, CR_{12}, CT_{21}, and CT_{12} should be smaller.

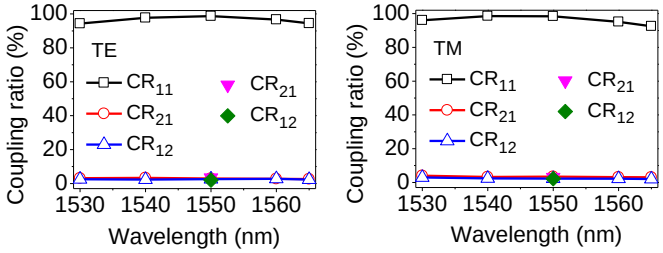

Fig. 9. Coupling ratios CR_{11}, CR_{21}, and CR_{12} for the TE and TM polarizations obtained from the power measurements over the C-band by selective mode excitation with a lensed fiber, where the data points for CR_{21} and CR_{12} at ~1550 nm were obtained from the power measurements by selective excitation of the E_{21} and E_{12} modes with an LPFG LP_{01}-LP_{11} mode converter.

We repeated the power measurements by using a CO_2-laser-written long-period fiber grating (LPFG) written in a two-mode fiber (OFS Fitel, LLC) [31] to selectively excite the E_{21} or E_{12} mode in Core 1. The LPFG was an LP_{01}-LP_{11} mode converter with a conversion efficiency higher than 99% (i.e., >20 dB) at ~1550 nm. The coupling ratios and the crosstalks at ~1550 nm, namely CR_{21}, CR_{12}, CT_{21}, and CT_{12},

obtained from the power measurements with the LPFG, were 3.4% (3.1%) and 2.0% (2.2%), −14.6 (−14.9), and −15.9 (−16.5) dB, respectively, for the TE (TM) polarizations. These data, which are also shown in Fig. 9 and Fig. 10, agree well with those obtained by using an offset and tilted lensed fiber for selective mode excitation.

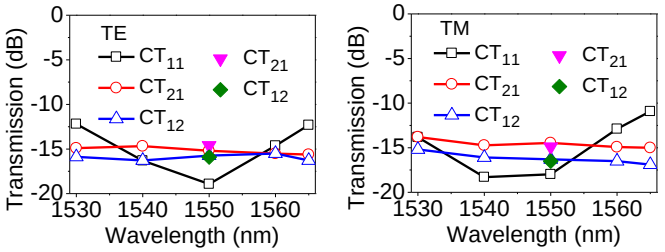

Fig. 10. Modal crosstalks CT_{11}, CT_{21}, and CT_{12} for the TE and TM polarizations obtained from the power measurements over the C-band by selective mode excitation with a lensed fiber, where the data points for CT_{21} and CT_{12} at ~1550 nm were obtained from the power measurements by selective excitation of the E_{21} and E_{12} modes with an LPFG LP_{01}-LP_{11} mode converter.

We measured the fiber butt-coupling losses of the device by comparing the output powers measured with and without connecting a short fiber to the core of concern at the output end of the device. We excited the individual modes at the input end by adjusting the position and the tilt angle of the laser beam and applied index-matching liquid to the fiber-waveguide interface to suppress the Fresnel reflection. In the C-band, the butt-coupling losses for the E_{11}, E_{21}, and E_{12} modes of Core 1 connected to a two-mode step-index fiber (OFS Fitel, LLC) were measured to be 0.9, 1.3, and 1.4 dB, respectively, and the butt-coupling loss for Core 2 connected to a standard SMF (SMF-28e, Corning) was 0.8 dB. By applying the cutback method to isolated reference cores of the same dimensions, the propagation losses of the E_{11}, E_{21} and E_{12} modes of Core 1 were measured to be 2.2, 2.4, and 2.5 dB/cm, respectively, and the propagation loss of the E_{11} mode of Core 2 was 2.0 dB/cm. All these losses were measured at 1550 nm. To measure the propagation losses of the high-order modes at 1550 nm, we used the LPFG mode converter to selectively excite the E_{21} or E_{12} mode. The insertion loss of the E_{11} mode from Core 1 to Core 2, which includes fiber butt-coupling losses at the two ends (assuming a two-mode fiber for Core 1 and a standard SMF for Core 2) was estimated to be 5.0 dB (calculated from the measured butt-coupling losses and the propagation losses of the reference waveguides at 1550 nm). However, the RIE-processed middle cladding in the fabricated device, which did not exist in the reference waveguides fabricated on the same substrate, could introduce significant additional losses. The actual insertion loss of the E_{11} mode in the fabricated device was measured to be 7.8 dB (at 1550 nm), which was larger than the estimated value. The insertion losses of the E_{21} and E_{12} modes were 6.2 and 6.6 dB, respectively. The insertion losses could be further reduced by using low-loss polymer materials [32], minimizing the use of RIE for thickness trimming, and using shorter lead waveguides at the two ends.

V. Conclusion

We have proposed a high-order-mode-pass mode (de)multiplexer based on a hybrid-core vertical DC, which allows the fundamental mode (i.e., the E_{11} mode) of an FMC to be coupled to an SMC without affecting the high-order modes of the FMC. We have designed and fabricated such a device with a three-mode core and an SMC with polymer material. Our experimental device, which has a length of 15 mm, provides a coupling ratio for the E_{11} mode higher than 92.5 % in the C-band with a relative residual power of the E_{11} mode in the three-mode core smaller than −10.9 dB. The modal crosstalks caused by the high-order modes are smaller than −13.8 dB in the C-band. The characteristics of the device are polarization-insensitive. Our device can realize the add-drop function for the fundamental mode and thus find applications in reconfigurable MDM systems, especially where (de)multiplexing of mode groups is required [33],[34]. The bandwidth of the device could be further extended by using tapered DC designs [35]. The hybrid-core vertical DC structure can be used to design a wide range of passive and active devices, such as mode group (de)multiplexers, mode-dependent-loss compensators, mode filters, dynamic mode add-drop multiplexers, mode switches, and mode routers. With our material system, there is room to design such a coupler with a longer length for a waveguide that supports more than three modes. By using a polymer system with a larger core-cladding index difference, it is possible to reduce the length of the device. This 3D structure substantially expands the capability of 3D polymer waveguide optics in the design of integrated mode-controlling devices for MDM applications.

References

[1] R.-J. Essiambre, G. Kramer, P. J. Winzer, G. J. Foschini, and B. Goebel, "Capacity limits of optical fiber networks," *J. Lightw. Technol.*, vol. 28, no. 4, pp. 662–701, Feb. 2010.

[2] D. J. Richardson, J. M. Fini, and L. E. Nelson, "Space-division multiplexing in optical fibres," *Nat. Photonics*, vol. 7, pp. 354–362, Apr. 2013.

[3] G. Li, N. Bai, N. Zhao, and C. Xia, "Space-division multiplexing: the next frontier in optical communication," *Adv. Opt. Photonics*, vol. 6, no. 4, pp. 413-487, Dec. 2014.

[4] T. Mizuno, H. Takara, A. Sano, and Y. Miyamoto, "Dense space-division multiplexed transmission," *J. Lightw. Technol.*, vol. 34, no. 2, pp. 582–592, Jan. 2016.

[5] T. Mizuno and Y. Miyamoto, "High-capacity dense space division multiplexing transmission," *Opt. Fiber Technol.*, vol. 35, pp. 108–117, Feb. 2017.

[6] D. Soma, Y. Wakayama, S. Beppu, S. Sumita, T. Tsuritani, T. Hayashi, T. Nagashima, M. Suzuki, M. Yoshida, K. Kasai, M. Nakazawa, H. Takahashi, K. Igarashi, I. Morita, and M. Suzuki, "10.16-peta-b/s dense SDM/WDM transmission over 6-mode 19-core fiber across the C+L band," *J. Lightw. Technol.*, vol. 36, no. 6, pp. 1362–1368, Mar. 2018.

[7] C. Koebele, M. Salsi, D. Sperti, P. Tran, P. Brindel, H. Mardoyan, S. Bigo, A. Boutin, F. Verluise, P. Sillard, M. Astruc, L. Provost, F. Cerou, G. Charlet, "Two mode transmission at 2×100 Gb/s over 40 km-long prototype few-mode fiber using LCOS-based programmable mode multiplexer and demultiplexer", *Opt. Express*, vol. 19, pp. 16593-16600, Aug. 2011.

[8] G. Labroille, B. Denolle, P. Jian, P. Genevaux, N. Treps, and J.-F. Morizur, "Efficient and mode selective spatial mode multiplexer based on multi-plane light conversion," *Opt. Express*, vol. 22, no. 13, pp. 15599–15607, Jun. 2014.

[9] K. Igarashi, D. Souma, T. Tsuritani, and I. Morita, "Selective mode multiplexer based on phase plates and Mach–Zehnder interferometer with image inversion function," *Opt. Express*, vol. 23, no. 1, pp. 183–194, Jan. 2015.
[10] A. M. Velazquez-Benitez, J. C. Alvarado, G. Lopez-Galmiche, J. E. Antonio-Lopez, J. Hernández-Cordero, J. Sanchez-Mondragon, P. Sillard, C. M. Okonkwo, and R. Amezcua-Correa, "Six mode selective fiber optic spatial multiplexer," *Opt. Lett.*, vol. 40, no. 8, pp. 1663–1666, Apr. 2015.
[11] S. G. Leon-Saval, N. K. Fontaine, J. R. Salazar-Gil, B. Ercan, R. Ryf, and J. Bland-Hawthorn, "Mode-selective photonic lanterns for space-division multiplexing," *Opt. Express*, vol. 22, no. 1, pp. 1036–1044, Jan. 2014.
[12] K. J. Park, K. Y. Song, Y. K. Kim, J. H. Lee, and Y. Kim, "Broadband mode division multiplexer using all-fiber mode selective couplers," *Opt. Express*, vol. 24, no. 4, pp. 3543–3549, Feb. 2016.
[13] S. H. Chang, S.-R. Moon, H. Chen, R. Ryf, N. K. Fontaine, K. J. Park, K. Kim, and A. J. K. Lee, "All-fiber 6-mode multiplexers based on fiber mode selective couplers," *Opt. Express*, vol. 25, no. 5, pp. 5734–5741, Mar. 2017.
[14] L. Han, S. Liang, H. Zhu, L. Qiao, J. Xu, and W. Wang, "Two-mode de/multiplexer based on multimode interference couplers with a tilted joint as phase shifter.," *Opt. Lett.*, vol. 40, no. 4, pp. 518–521, Feb. 2015.
[15] C. Sun, Y. Yu, G. Chen, and X. Zhang, "Integrated switchable mode exchange for reconfigurable mode-multiplexing optical networks," *Opt. Lett.*, vol. 41, no. 14, pp. 3257–3260, Jul. 2016.
[16] K. Saitoh, T. Uematsu, N. Hanzawa, Y. Ishizaka, K. Masumoto, T. Sakamoto, T. Matsui, K. Tsujikawa, and F. Yamamoto, "PLC-based LP_{11} mode rotator for mode-division multiplexing transmission," *Opt. Express*, vol. 22, no. 16, pp. 19117–19130, Aug. 2014.
[17] K. Saitoh, N. Hanzawa, T. Sakamoto, T. Fujisawa, Y. Yamashita, T. Matsui, K. Tsujikawa, and K. Nakajima, "PLC-based mode multi/demultiplexers for mode division multiplexing," *Opt. Fiber Technol.*, vol. 35, pp. 80–92, Feb. 2017.
[18] W. Jin and K. S. Chiang, "Three-dimensional long-period waveguide gratings for mode-division-multiplexing applications," *Opt. Express*, vol. 26, no. 12, pp. 15289-15299, Jun. 2018.
[19] J. D. Love and N. Riesen, "Mode-selective couplers for few-mode optical fiber networks," *Opt. Lett*., vol. 37, no. 19, pp. 3990-3992, Oct. 2012.
[20] J. Dong, K. S. Chiang, and W. Jin, "Mode multiplexer based on integrated horizontal and vertical polymer waveguide couplers," *Opt. Lett.*, vol. 40, no. 13, pp. 3125–3128, Jul. 2015.
[21] J. Dong, K. S. Chiang, and W. Jin, "Compact three-dimensional polymer waveguide mode multiplexer," *J. Lightw. Technol.*, vol. 33, no. 22, pp. 4580–4588, Nov. 2015.
[22] T. Watanabe and Y. Kokubun, "Demonstration of mode-evolutional multiplexer for few-mode fibers using stacked polymer waveguide," *IEEE Photon. J.*, vol. 7, no. 6, Art. no. 7103311, Dec. 2015.
[23] N. Riesen, S. Gross, J. D. Love, and M. J. Withford, "Femtosecond direct-written integrated mode couplers," *Opt. Express*, vol. 22, no. 24, pp. 29855–29861, Dec. 2014.
[24] Y. Wu and K. S. Chiang, "Ultra-broadband mode multiplexers based on three-dimensional asymmetric waveguide branches," *Opt. Lett*., vol. 42, no. 3, pp. 407-410, Feb. 2017.
[25] Q. Huang, Y. Wu, W. Jin, and K. S. Chiang, "Mode multiplexer with cascaded vertical asymmetric waveguide directional couplers," *J. Lightw. Technol.*, vol. 36, no. 14, pp. 2903–2911, Jul. 2018.
[26] Q. Huang, W. Jin, and K. S. Chiang, "Broadband mode switch based on three-dimensional waveguide Mach-Zehnder interferometer," *Opt. Lett*. vol. 42, no. 23, pp. 4877-4880, Dec. 2017.
[27] Q. Huang, Y. Wu, W. Jin, and K. S. Chiang, "Broadband mode router based on three-dimensional Mach-Zehnder interferometer and waveguide branches," *Proc. CLEO 2018*, Paper STh1A.2.
[28] Q. Huang, K. S. Chiang, and W. Jin, "Thermo-optically controlled vertical waveguide directional couplers for mode-selective switching," *IEEE Photon. J.*, vol. 10, no. 6, Art. no. 6602714, Dec. 2018.
[29] Y. Wang, K. Chen, L. Wang, and K. S. Chiang, "Sidewall-grating-assisted polymer-waveguide directional coupler for forward coupling of fundamental modes," *Proc. Asia Communications and Photonics Conference*, 2015, Paper ASu3A.3.
[30] X. Zi, L. Wang, K. Chen, and K. S. Chiang, "Mode-selective switch based on thermo-optic asymmetric directional coupler," *IEEE Photon. Technol. Lett*., vol. 30, no. 7, pp. 618–621, Apr. 2018.
[31] J. Dong and K. S. Chiang, "Temperature-insensitive mode converters with CO2-laser written long-period fiber gratings," *IEEE Photon. Technol. Lett.*, vol. 27, no. 9, pp. 1006–1009, May 2015.
[32] D. de Felipe, M. Kleinert, C. Zawadzki, A. Polatynski, G. Irmscher, W. Brinker, M. Moehrle, H. G. Bach, N. Keil, and M. Schell, "Recent developments in polymer-based photonic components for disruptive capacity upgrade in data centers," *J. Lightw. Technol.* vol. 35, no. 4, pp. 683–689, Feb. 2017.
[33] K. Benyahya, C. Simonneau, A. Ghazisaeidi, P. Jian, J.-F. Morizur, G. Labroille, M. Bigot, P. Sillard, J. Renaudier, and G. Charlet, "High-speed bi-directional transmission over multimode fiber link in IM/DD Systems," *J. Lightw. Technol.*, vol. 36, no. 18, pp. 4174–4180, Sep. 2018.
[34] K. Benyahya, C. Simonneau, A. Ghazisaeidi, N. Barre, P. Jian, J.-F. Morizur, G. Labroille, M. Bigot, P. Sillard, J. G. Provost, H. Debregeas, J. Renaudier, and G. Charlet, "Multiterabit transmission over OM2 multimode fiber with wavelength and mode group multiplexing and direct detection," *J. Lightw. Technol.*, vol. 36, no. 2, pp. 355–360, Jan. 2018.
[35] N. Riesen and J. D. Love, "Ultra-broadband tapered mode-selective couplers for few-mode optical fiber networks," *IEEE Photon. Technol. Lett.*, vol. 25, no. 24, pp. 2501–2504, Dec. 2013.

Quandong Huang received his B.E. degree in electronic science and technology and M.E. degree in optics from Shenzhen University in 2012 and 2015, respectively. He is currently pursuing the Ph.D. degree at the City University of Hong Kong. His research interests include fiber optics and waveguide devices for mode-division multiplexing.

Kin Seng Chiang (M'94) received the B.E. (Hons. I) and Ph.D. degrees in electrical engineering from the University of New South Wales, Sydney, N.S.W., Australia, in 1982 and 1986, respectively.

In 1986, he spent six months with the Department of Mathematics, Australian Defense Force Academy, Canberra, A.C.T., Australia. From 1986 to1993, he was with the Division of Applied Physics, Commonwealth Scientific and Industrial Research Organization, Sydney, N.S.W., Australia. From 1987 to 1988, he received a Japanese Government research award and spent six months at the Electrotechnical Laboratory, Tsukuba City, Japan. From 1992 to 1993, he worked concurrently for the Optical Fibre Technology Centre, University of Sydney. In August 1993, he joined the Department of Electronic Engineering, City University of Hong Kong, Kowloon Tong, Hong Kong, where he is currently a Chair Professor. From 2007 to 2010, he was concurrently a Chang Jiang Chair Professor of the University of Electronic Science and Technology of China (UESTC) and is currently associated with UESTC under the National Thousand Talents Program. He has published more than 500 papers on optical fiber/waveguide theory and modeling, fiber/waveguide characterization, fiber/waveguide devices, optical sensors, optical interconnect, and nonlinear guided-wave optics. He served as an Associate Editor of *Journal of Lightwave Technology* during 2009–2014, and is currently an editor of *Light: Science & Applications*.

Dr. Chiang is a fellow of the Optical Society (OSA), a member of the International Society for Optical Engineering (SPIE), and the Australian Optical Society. He received the Croucher Senior Research Fellowship for 2000–2001.